remote sensing

Technical Note

Ground-Based SAR Moving Target Refocusing Based on Relative Speed for Monitoring Mine Slopes

Wenjie Shen , Shuo Wang, Yun Lin , Yang Li, Fan Ding and Yanping Wang *

Radar Monitoring Technology Laboratory, School of Information Science and Technology, North China University of Technology, Beijing 100144, China
* Correspondence: wangyp@ncut.edu.cn

Abstract: Ground-based synthetic aperture radar (GBSAR) has the advantage of retrieving submillimeter deformation of the mine slope by using the differential interferometry technique, which is important for safe production in mining applications. However, the moving vehicle's defocus/displaced signal will mask the SAR image of the mining area which affects the accuracy of interference phase extraction and deformation inversion. In order to remove its influence, the moving target can first be refocused and then removed. To our knowledge, there is no GBSAR moving target refocusing method currently. Hence, the refocusing method is necessary. To solve the above problem, this paper proposes a single-channel FMCW-GBSAR moving target refocusing method based on relative speed. Firstly, the FMCW-GBSAR moving target signal model is analyzed, and then the relative speed based signal model is deduced. Based on the model and GBSAR's feature of incomplete synthetic aperture, the Range Doppler (RD) algorithm is adopted and improved to achieve refocusing using relative speed parameters. The algorithm is controlled by relative speed and squint angle; thus, the refocused target image can be obtained via searching 2D parameters. The proposed method is verified by the synthetic data, which are generated by combining NCUT FMCW GBSAR real data and simulated moving target echo.

Keywords: ground-based synthetic aperture radar; relative speed; moving target refocusing; range doppler algorithm

Citation: Shen, W.; Wang, S.; Lin, Y.; Li, Y.; Ding, F.; Wang, Y. Ground-Based SAR Moving Target Refocusing Based on Relative Speed for Monitoring Mine Slopes. *Remote Sens.* **2022**, *14*, 4243. https://doi.org/10.3390/rs14174243

Academic Editors: Guang-Cai Sun, Gang Xu, Jianlai Chen and Jixiang Xiang

Received: 19 July 2022
Accepted: 26 August 2022
Published: 28 August 2022

1. Introduction

Mining slope stability monitoring and deformation information acquisition are directly related to production safety. Ground-based synthetic aperture radar (GBSAR) combined with differential interferometry technique can achieve submillimeter deformation information retrieval after around a minute. It has become an effective tool for slope deformation monitoring [1,2]. The accuracy of deformation retrieval relies on high coherence of GBSAR image stack. However, the moving vehicles in the mining area will generate lots of defocused/displaced signatures on the SAR image, which can cause decoherence. Hence, such phenomenon reduces the accuracy of deformation inversion. One feasible way to eliminate the influence is to remove the refocused moving target. Under a refocused state, the moving targets only occupy a very small area, such as several pixels. Then, they can be removed with minimal information loss of the static mine slope scene. Currently, the frequency modulated continuous wave (FMCW) system is widely used in GBSAR, and there is no moving target refocusing for GBSAR (to our knowledge). Therefore, as a research foundation for removing the above influence, the moving target refocusing method for FMCW-GBSAR is necessary.

Due to the moving target's motion-induced imaging parameter mismatch, there is a defocusing effect in SAR images. The moving target imaging aims at obtaining the well focused target signature. The well refocusing relies on compensation for target motion-induced three terms (range walk, range curvature, quadratic and higher phase term).

Typical methods include two kinds, the keystone transform-based methods and SAR imaging algorithm-based methods. The keystone transformation was first proposed by Perry [3]. It can remove range walk without prior knowledge of moving target range motion. However, the original method can only correct range walk and the transformation will affect the quadratic phase term. The improved and modified method can be found in [4–7]. The other kind is to modify the current SAR imaging method [8–14]. The most typical idea is based on the relative speed method, which was first introduced by Jao [9]. By constructing a relative speed-based moving target signal model, the moving target signal model is equal to the stationary target model. A new efficient algorithm for refocusing of ground fast-maneuvering targets is presented by [13]. Another new idea for SAR imaging of moving target using range azimuth joint processing (RAJP) is presented by Shu [14]. Thus, the existing imaging algorithm can be fully utilized. However, the above methods are usually used for airborne and spaceborne pulsed SAR systems. Ground-based SAR usually uses the FMCW radar system, i.e., FMCW-SAR, due to the cost and near-range imaging need.

The main difference in FMCW SAR is that the "stop-go-stop" model is not applicable, due to the continuous signal transmitting and receiving. In recent years, the FMCW-SAR algorithms for stationary scene are relatively matured such as Range Doppler (RD), Frequency Scaling (FS), Polar Format Algorithm (PFA) and Omega-K (ωK) [15–26]. Thus, developing a relative speed-based FMCW-SAR moving target imaging method is a viable option, as for airborne platform in [27]. However, the key difference in GBSAR is the incomplete synthetic aperture feature caused by limit rail length, so it is not readily applicable to FMCW-GBSAR. Another difference is that the GBSAR moves slower than moving vehicle, which is different from fact that moving vehicle moves slower than airborne and spaceborne SAR. The above facts make researchers reconsider and analyze the relative speed-based signal model.

To solve the above problems, this paper proposes a moving target imaging algorithm based on relative speed for FMCW-GBSAR. The FMCW-GBSAR moving target signal model is analyzed, and relative speed-based signal model is deduced. Based on the model and the incomplete synthetic aperture of GBSAR, the Range Doppler (RD) algorithm is adopted and improved. The key modification in RD is adding the time domain phase compensation step in azimuth compression to achieve refocusing. The algorithm is controlled by relative speed and squint angle; thus, the refocused target image can be obtained via searching 2D parameters. The proposed method is verified by the synthetic data, which are generated by combining NCUT FMCW GBSAR real data and simulated moving target echo.

The rest of the paper is organized as follows. Section 2 analyzes the FMCW-GBSAR moving target signal model, which shows that the complexity of developing the imaging algorithm based on this model. Section 3 gives the relative speed-based signal model, and the relationship between radar velocity and moving target velocity is analyzed. The four detail conditions due to the fact that moving target speed faster than GBSAR are also presented in this section. In the Section 4, the moving target imaging algorithm based on relative speed signal model is introduced in detail. The algorithm improves the RD algorithm to suit for GBSAR. Section 5 is the experiment. Last is conclusion.

2. Moving Target Signal Model

Figure 1 shows the geometry when azimuth time $t = 0$. Y-axis is the azimuth direction that the radar moves along with constant speed v_s; x-axis is the range direction; the origin O is the rail's midpoint. Radar position is $(0, v_s t)$. v_a and v_r are the velocities of the moving target in azimuth and range, respectively. The moving target is at P (x_0, y_0) when $t = 0$, and its velocity is (v_r, v_a). The moving target's motion can be expressed as $(x_0 + v_r t, y_0 + v_a t)$. Here, we assume the moving target speed does not exceed the Pulse Repetition Frequency (PRF), i.e., no Doppler ambiguity occurs. Due to stop-and-go, approximation is not valid in FMCW SAR [28–30]. Above, t is given as $t = t_a + t_r$, where t_a and t_r are the azimuth and range time, respectively.

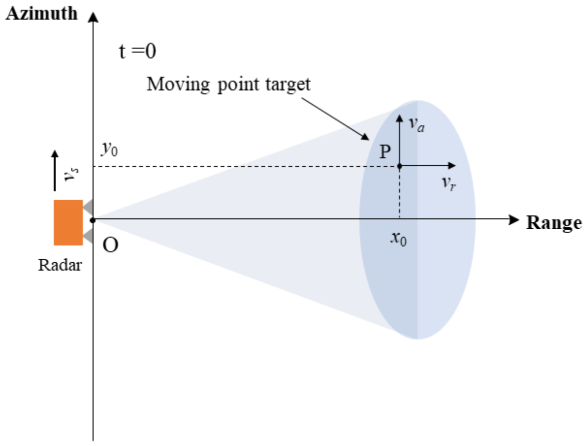

Figure 1. Geometry of the GBSAR and moving target.

As in Figure 1, the range equation is given as:

$$R(t) = \sqrt{(x_0 + v_r t)^2 + (y_0 + (v_a - v_s)t)^2} \tag{1}$$

The received signal after dechirp processing is:

$$\begin{aligned} S(t_r, t_a) = A \cdot \exp\left[-j\tfrac{4\pi}{\lambda} R(t_r, t_a)\right] \cdot \exp\left[j\tfrac{4\pi K_r}{c^2}\left(R(t_r, t_a) - R_{ref}\right)^2\right] \\ \exp\left[-j\tfrac{4\pi}{c} K_r \left(R(t_r, t_a) - R_{ref}\right)\left(t_r - \tfrac{2R_{ref}}{c}\right)\right] \end{aligned} \tag{2}$$

In the formula, A is the complex constant and window functions in azimuth and range which will be neglected in paper's following deduction. λ is wavelength, c is the speed of light, K_r is the chirp rate and R_{ref} is the reference range which typically selects scene center.

Apply Taylor expansion to Equation (1) at $t = 0$ and omit the higher order terms:

$$\begin{cases} R(t) \approx \frac{R(0)}{0!} + \frac{R'(0)}{1!}(t-0) + \frac{R''(0)}{2!}(t-0)^2 = R(0) + R'(0) \cdot t + \frac{R''(0)}{2} \cdot (t)^2 \\ R(0) = \sqrt{x_0^2 + y_0^2} \\ R'(0) = (x_0^2 + y_0^2)^{-\frac{1}{2}} \cdot (v_r x_0 + (v_a - v_s) y_0) \\ R''(0) = \left(v_r^2 + (v_a - v_s)^2\right)) \cdot (x_0^2 + y_0^2)^{-\frac{1}{2}} - (x_0^2 v_r^2 + y_0^2 (v_a - v_s)^2) \cdot (x_0^2 + y_0^2)^{-\frac{3}{2}} \end{cases} \tag{3}$$

Substitute $t = t_a + t_r$ into Equation (3), since the focusing effect is mainly related to the quadratic term of t_a, so the quadratic term of t_r can be omitted [31] and we can obtain a simplified formula as:

$$\begin{aligned} R(t_r, t_a) &\approx R(0) + R'(0) \cdot (t_r + t_a) + \frac{R''(0)}{2} \cdot (t_r + t_a)^2 \\ &= R(0) + R'(0) \cdot (t_r + t_a) + \frac{R''(0)}{2} \cdot (t_r^2 + t_a^2 + 2t_r t_a) \\ &\approx R(0) + R'(0) \cdot (t_r + t_a) + \frac{R''(0)}{2} \cdot (t_a^2 + 2t_r t_a) \end{aligned} \tag{4}$$

Rewrite Equation (2) with Equation (4), and the signal can be expressed as:

$$\begin{aligned} s(t_r, t_a) &= \exp\left(-j\tfrac{4\pi}{\lambda}\left(R(0) + \tfrac{R''(0)}{2} t_a^2\right)\right) \cdot \exp\left[j\tfrac{4\pi K_r}{c^2}\left(R''(0) - R_{ref}\right)^2\right] \cdot \\ &\exp\left(-j\tfrac{4\pi}{\lambda} \cdot R''(0) \cdot t_r t_a\right) \cdot \exp\left(j\tfrac{4\pi}{\lambda} \cdot R'(0) \cdot t_a\right) \cdot \exp\left(j\tfrac{4\pi}{\lambda} \cdot R'(0) \cdot t_r\right) \cdot \\ &\exp\left[-j\tfrac{4\pi}{c} K_r \left(R(0) + R'(0) \cdot t_a + \tfrac{R''(0)}{2} \cdot t_a^2 - R_{ref}\right)\left(t_r - \tfrac{2R_{ref}}{c}\right)\right] \end{aligned} \tag{5}$$

Recall the expression of $R(0)$, $R'(0)$ and $R''(0)$; if they are substituted into Equation (5), the expression of moving target signal can be obtained. The expression of Equation (5) replaced with all terms is listed in the Appendix A. It can be seen that the moving target signal model in FMCW-SAR is quite complex. To obtain a well focused image, it is necessary to compensate each exponential term. Each parameter should be tuned for refocusing which makes the algorithm complex and time-consuming.

In the next section, we introduce relative speed to simplify the moving target signal model. It can be seen that the relative speed-based moving target signal model is equal to the static target signal model. In that model, only one parameter of relative speed needs to be tuned. Therefore, the existing imaging algorithm can be fully utilized, and its complexity can be reduced.

3. Relative Speed-Based Moving Target Signal Model

3.1. Relative Speed Transformation

In this section, the relative speed-based moving target signal model is derived and analyzed. Figure 2 shows the geometry after relative speed transformation when azimuth time $t = 0$. The radar position changes from $(0, v_s t)$ to $(0, v'_s t)$. The moving target is at P (x_0, y_0) when $t = 0$, its velocity is (v_r, v_a). After relative speed transformation, the moving target P rotates θ to P′ as a stationary target. The target position changes from $(x_0 + v_r t, y_0 + v_a t)$ to (x'_0, y'_0).

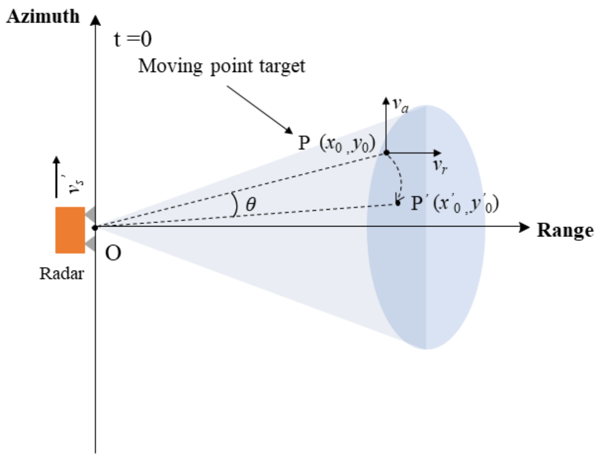

Figure 2. Geometry of the GBSAR and moving target after relative speed transformation.

Equations (6) and (7) are relative speed transformation, v'_s is the value of relative speed, θ shows its direction. According to the aforementioned geometry and motion assumptions, the v'_s and θ are constant.

$$v'_s = \sqrt{(v_s - v_a)^2 + (v_r)^2} \tag{6}$$

$$\theta = \arctan\left(\frac{|v_r|}{|v_s - v_a|}\right) \tag{7}$$

Applying Equations (6) and (7) to Equation (1) with proper mathematical deduction, we can rewrite range equation as Equation (8).

$$R(t) = \sqrt{(x_0 \cos\theta - y_0 \sin\theta)^2 + ((x_0 \sin\theta + y_0 \cos\theta) - v_s' t)^2} \tag{8}$$

Since (x_0, y_0) are also constant, and x'_0 and y'_0 in Equation (9) are used to simplify Equation (8) as shown in Equation (10).

$$\begin{cases} x'_0 = x_0 \cos\theta - y_0 \sin\theta \\ y'_0 = x_0 \sin\theta + y_0 \cos\theta \end{cases} \tag{9}$$

$$R(t) = \sqrt{(x'_0)^2 + (y'_0 - v'_s t)^2} \tag{10}$$

By examining Equation (10), we can find its form is equal to the stationary target's range equation formula. This can be seen by setting v_r and v_a in Equation (1) as zero, which is shown below.

$$R(t) = \sqrt{(x_0)^2 + (y_0 - v_s t)^2} \tag{11}$$

Comparing Equations (10) and (11), we can find that after the relative speed transformation, the moving target range equation is equal to the stationary target's formula. Hence, the current imaging method can be utilized with minor modification, which reduces complexity. The difference is that target position is projected from (x_0, y_0) to (x'_0, y'_0). The new position is determined by relative speed's value and direction based on rotation formula (9).

3.2. Analysis on Relative Speed Model

As in Equation (10), it is clear that the moving target is projected as a stationary target at (x'_0, y'_0). We can find that it is the squinted SAR imaging model, which make it is easier to link the current imaging method. This subsection conducts the analysis on the relative speed model with squint angle.

The geometry of radar and moving target is shown in Figure 3. The origin O is the rail's midpoint, O′ is the position of radar at time t and P′ is the position of moving target after relative speed transformation. O′P′ is the range between the radar and the target at arbitrary time, and R_0 is the range between the target and radar at $t = 0$. Additionally, θ' is the squint angle at $t = 0$.

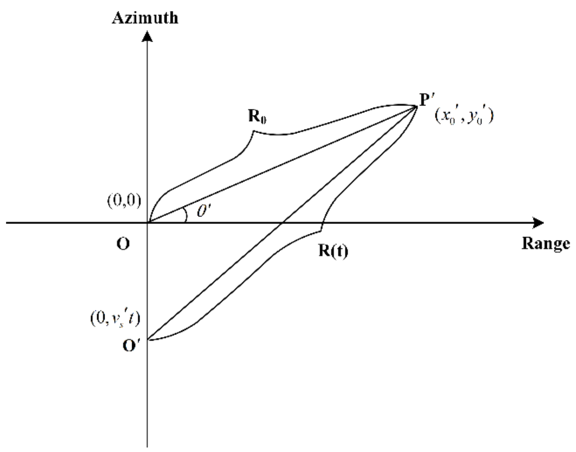

Figure 3. Geometric model of moving target based on relative speed.

From Figure 3, we can obtain $R_0 = \sqrt{(x'_0)^2 + (y'_0)^2}$ and $\theta' = \arctan\frac{y'_0}{x'_0}$. Based on the law of cosines, the range equation can be expressed as:

$$R(t) = \sqrt{(v'_s t)^2 + R_0^2 - 2R_0 v'_s t \sin\theta'} \tag{12}$$

Since the GBSAR system uses the FMCW signal, replace $t = t_r + t_a$ into Equation (12) to obtain Equation (13).

$$R(t_r, t_a) = \sqrt{(v'_s t_a + v'_s t_r)^2 + R_0^2 - 2R_0(v'_s t_a + v'_s t_r)\sin\theta'} \tag{13}$$

Then, the received signal is rewritten as follows:

$$\begin{aligned} s(t_r, t_a) &= \exp\left[-j\frac{4\pi}{\lambda}R(t_r, t_a)\right] \\ &\cdot \exp\left[-j\frac{4\pi}{\lambda}K_r\left(R(t_r, t_a) - R_{ref}\right)\left(t_r - \frac{2R_{ref}}{c}\right)\right] \\ &\cdot \exp\left[-j\frac{4\pi K_r}{c^2}\left(R(t_r, t_a) - R_{ref}\right)^2\right] \end{aligned} \tag{14}$$

T_p is the duration of transmitted signal, and the fast time t_r is $|t_r| \le T_p/2$. The third exponential term is RVP (residual video phase term). This item can be compensated according to reference [32].

Since the range equation in Equation (13) is related to the fast time, we expand the slant range $R(t_r, t_a)$ at $t_r = 0$ by Taylor expansion and ignore higher order term to obtain Equation (15).

$$\begin{aligned} R(t_r, t_a) &= \sqrt{(v'_s t_r + v'_s t_a)^2 + R_0^2 - 2R_0(v'_s t_r + v'_s t_a)\sin\theta'} \\ &\approx \sqrt{(v'_s t_a)^2 + R_0^2 - 2R_0 v'_s t_a \sin\theta'} + \frac{(v'_s)^2 t_a - R_0 v'_s \sin\theta'}{\sqrt{(v'_s t_a)^2 + R_0^2 - 2R_0 v'_s t_a \sin\theta'}} t_r \end{aligned} \tag{15}$$

Let $R(t_a) = \sqrt{R_0^2 + (v'_s)^2 t_a^2 - 2R_0 v'_s t_a \sin\theta'}$, then apply Taylor expansion at $t_a = 0$ and ignore the high order term:

$$\begin{aligned} R(t_a) &= \sqrt{R_0^2 + (v'_s)^2 t_a^2 - 2R_0 v'_s \sin\theta'} \\ &\approx R_0 - v'_s \sin\theta' t_a + \frac{(v'_s)^2\cos^2\theta'}{2R_0} t_a^2 \end{aligned} \tag{16}$$

Among them, $-v'_s \sin\theta' t_a$ causes linear range walk and Doppler centroid shift, denoted as $\Delta R(t_a)$. During the imaging process, the influence of the linear range walk and Doppler centroid shift should be corrected.

Substitute Equation (15) with (16), the range equation is:

$$R(t_r, t_a) \approx R_a(t_a) + \frac{(v'_s)^2 t_a - R_0 v'_s \sin\theta'}{R_a(t_a)} t_r \tag{17}$$

By substituting Equation (17) into (14), the echo model of the signal can be simplified as:

$$\begin{aligned} S\prime(t_r, t_a) &= \exp\left\{-j\frac{4\pi}{\lambda}\left(R_0 + \frac{(v'_s)^2\cos^2\theta'}{2R_0}t_a^2\right)\right\} \\ &\cdot \exp\left\{-j\frac{4\pi}{\lambda}\frac{(v'_s)^2 t_a - R_0(v'_s)\sin\theta'}{R_a(t_a)}t_r\right\} \\ &\cdot \exp\left\{-j\frac{4\pi}{c}K_r\left[R_a(t_a) + \frac{(v'_s)^2 t_a - R_0 v'_s \sin\theta'}{R_a(t_a)}t_r - R_{ref}\right]\left(t_r - \frac{2R_{ref}}{c}\right)\right\} \end{aligned} \tag{18}$$

The analysis of signal model in Equation (18) shows that the first exponential term causes azimuth defocusing [33]. The second exponential term is a Doppler shift caused by the continuous motion of the radar. Since the Doppler shift will bring the migration through range cell to the echo envelope and result in azimuth defocusing during the imaging process [34], the impact of this item should be eliminated in processing.

3.3. Analysis of Searching Refocusing Parameters

It can be seen from Section 3.2 that the moving target can be refocused by tuning parameters v'_s and θ'. Therefore, this section analyzes 2D parameters searching based on v'_s and θ'. Firstly, as can be seen from Figure 3, θ' is the squint angle at $t = 0$. So, based on the prior of beam pointing direction, the search range of θ' is $|\theta'| < 90^{\circ}$.

Next, we discuss the tuning of relative speed parameter v'_s. Because the GBSAR moves slower than moving target speed due to it being constrained to the rail (typically as cm/s level). It should consider both value and direction. It has four cases when considering the situations of target-radar speed difference. The four cases are listed in Figure 4. Here, the positive speed value means the target speed direction along the positive axis.

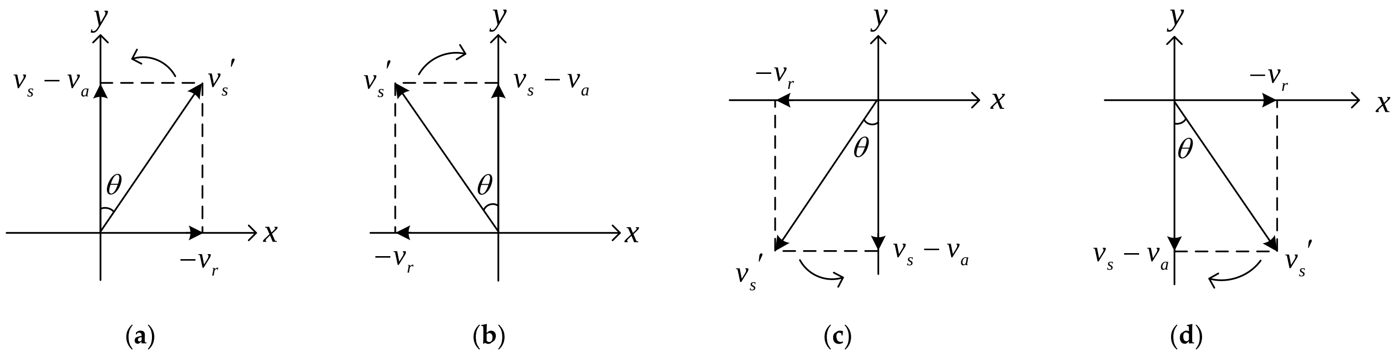

Figure 4. Relative speed's four cases due to speed difference. (**a**) $v_s - v_a > 0$,$v_r < 0$. (**b**) $v_s - v_a > 0$, $v_r > 0$. (**c**) $v_s - v_a < 0$,$v_r > 0$. (**d**) $v_s - v_a < 0$,$v_r < 0$.

From Figure 4a,b, when $v_s - v_a > 0$, v'_s can be calculated by $\sqrt{(v_s - v_a)^2 + (v_r)^2}$. From Figure 4c,d, when $v_s - v_a < 0$, v'_s can be calculated by $-\sqrt{(v_s - v_a)^2 + (v_r)^2}$. Additionally, as denoted in Equation (7), the rotation angle θ will change according to the direction of the resultant velocity v'_s. So, the search range of v'_s is $|v'_s| < v_m$, where v_m is the maximum relative speed for refocusing, which can be set according to the practical needs in application.

Here, the two-dimensional parameters' searching strategy is not discussed due to it not being the scope of this paper, and it will be studied in the future.

4. Refocus Imaging Algorithm

Figure 5 is a flowchart of the proposed refocusing imaging algorithm, which mainly includes the three parts: (1) The 2-dimensional parameters search space (v'_s, θ') is first established. (2) In each parameters search loop, the modified RD algorithm is applied to the input data. The modified RD method contains linear range migration correction, Doppler centroid correction, range cell migration correction, Doppler shift correction and azimuth compression. (3) When target is refocused, the iteration loop stops, and the refocused target image is output.

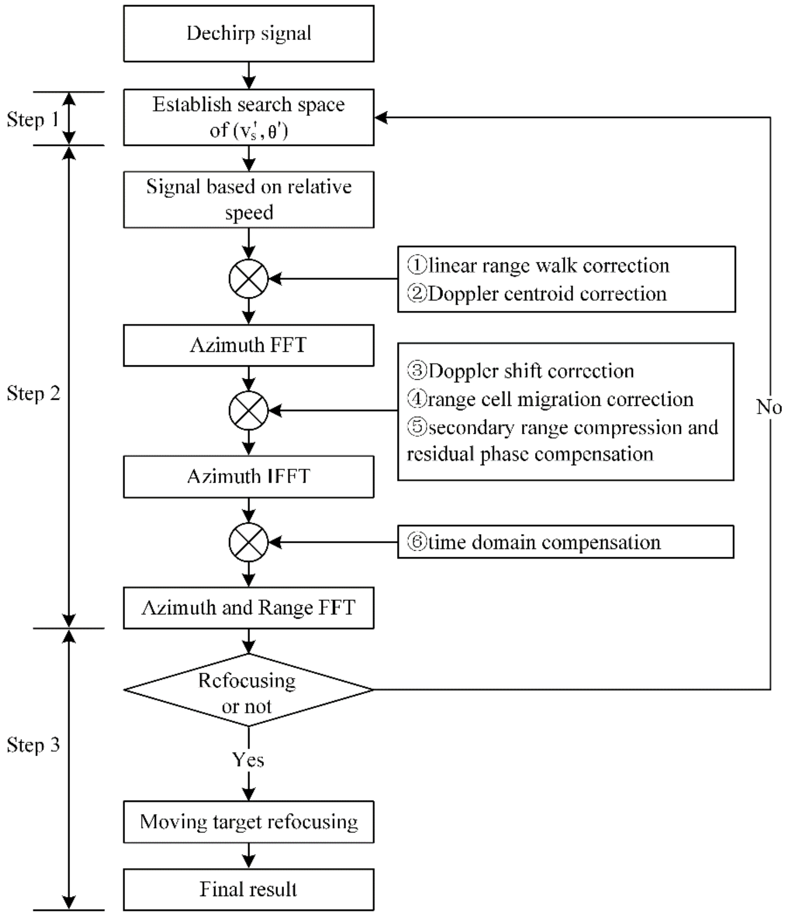

Figure 5. Flowchart of the proposed refocusing method.

As mentioned in Equation (16), $-v'_s \sin\theta' t_a$ causes linear range walk and Doppler centroid, denoted as $\Delta R(t_a)$. The Doppler centroid and linear range walk can be corrected by multiplying the Equation (18) with (19):

$$H_{dc} = \exp\left\{ j\frac{4\pi}{c} K_r \Delta R(t_a) \left(t_r - \frac{2R_{ref}}{c} \right) + j\frac{4\pi}{\lambda} \Delta R(t_a) \right\} \tag{19}$$

Then, based on the stationary phase principle, Equation (18) after linear range walk correction in Doppler domain is:

$$\begin{aligned} S'(t_r, f_a) &= \exp\left\{ -j\tfrac{4\pi}{\lambda} R_0 \beta(f_a) \right\} \cdot \exp\left\{ -j\tfrac{4\pi K_r}{c} \left[\tfrac{R_0}{\beta(f_a)} - R_{ref} \right] \left(t_r - \tfrac{2R_{ref}}{c} \right) \right\} \\ &\cdot \exp\left\{ -j\tfrac{2\pi\lambda K_r^2 R_0}{c^2} \tfrac{\beta^2(f_a)-1}{\beta^3(f_a)} \left(t_r - \tfrac{2R_{ref}}{c} \right)^2 \right\} \\ &\cdot \exp\{ j2\pi f'_{dc} t_r \} \cdot \exp\left\{ j\tfrac{2\pi \sin\theta' R_0 f_a^3}{\lambda \cos\theta' \left(f_{aM}^2 - f_a^2 \right)^{3/2}} \right\} \end{aligned} \tag{20}$$

In Equation (20), $f_{aM} = -\frac{2v'_s}{\lambda}$, and the Doppler centroid is $f'_{dc} = \frac{2v'_s \sin\theta'}{\lambda}$. Since the Doppler shift caused by the continuous motion of radar should be corrected, the Doppler shift correction function is:

$$H_{dfs} = \exp\left[-j2\pi f'_{dc} t_r \right] \tag{21}$$

The $\beta(f_a)$ in Equation (20) is the RCMC correction factor as shown in Equation (22):

$$\beta(f_a) = \sqrt{1 - \left(\frac{\lambda f_a}{2v'_s \cos\theta'} \right)^2} \tag{22}$$

Similar to [14], we use the following approximation (23):

$$\frac{R_0}{\beta(f_a)} \approx R_0 + \frac{1}{2} R_0 \frac{\lambda^2 f_a^2}{4(v'_s)^2 \cos^2 \theta'} \tag{23}$$

The corresponding range cell migration correction function is as following:

$$H_{rcmc} = \exp\left\{ j \frac{4\pi K_r}{c} \frac{1}{2} R_0 \frac{\lambda^2 f_a^2}{(2v'_s \cos\theta')^2} \left(t_r - \frac{2R_{ref}}{c} \right) \right\} \tag{24}$$

The third exponential term in Equation (20) is a function of fast time, which provides a second range compression function:

$$H_{src} = \exp\left\{ j \frac{2\pi\lambda K_r^2 R_0}{c^2} \frac{\beta^2(f_a) - 1}{\beta^3(f_a)} \left(t_r - \frac{2R_{ref}}{c} \right)^2 \right\} \tag{25}$$

Next, compensate the last term using H_{f_a} in the Doppler domain as Equation (26):

$$H_{f_a} = \exp\left\{ -j \frac{2\pi \sin\theta' R_0 f_a^3}{\lambda \cos\theta' \left(f_{aM}^2 - f_a^2\right)^{3/2}} \right\} \tag{26}$$

The echo signal can be expressed as:

$$S'(t_r, f_a) = \exp\left\{ -j \frac{4\pi}{\lambda} R_0 \beta(f_a) \right\} \cdot \exp\left\{ -j \frac{4\pi K_r}{c} \left[R_0 - R_{ref} \right] \left(t_r - \frac{2R_{ref}}{c} \right) \right\} \tag{27}$$

By using azimuth inverse FFT and range FFT, the signal can be expressed as:

$$S'(f_r, t_a) = \sin c\left\{ \pi T_p \left[f_r + \frac{2K_r}{c} \left(R_0 - R_{ref} \right) \right] \right\} \cdot \exp\left\{ -j \frac{4\pi R_{ref}}{c} f_r \right\} \cdot \exp\left\{ -j \frac{4\pi}{\lambda} \left(R_0 + \frac{(v'_s)^2 \cos^2\theta'}{2R_0} t_a^2 \right) \right\} \tag{28}$$

The remaining exponential term in Equation (28) is the phase history in the azimuth time domain, which controls azimuth focusing. It is easy to find the quadratic phase in this term. Due to the incomplete synthetic aperture feature in GBSAR, the imaging scene is imaged in the Doppler domain; thus, this quadratic phase term will cause target azimuth defocusing. The compensation term is therefore given as Equation (29).

$$H_{ref} = \exp\left(j \frac{4\pi}{\lambda} \left(\frac{(v'_s)^2 \cos^2\theta'}{2R_0} t_a^2 \right) \right) \tag{29}$$

After applied Fourier transform along azimuth direction, the target image can be obtained. By evaluating the parameter of contrast, the refocusing state of target can be obtained. If the maximum contrast is reached, then the focusing target image is output as the final result.

For different moving targets, the values of v'_s and θ' for refocusing are different. When the values of v'_s and θ' are determined, only the moving targets with matching parameters can be refocused. The targets that do not match will be defocused. For these mismatched moving targets, the greater the difference between true parameters and processing parameters, the more serious the defocusing will be in the image.

5. Experiments

In this section, the experiments of point target simulation and synthetic data are introduced, respectively.

5.1. Point Target Simulation

Table 1 shows the system parameters used in simulation, which are extracted from the real system of NCUT's GBSAR system. It works in 17 GHz, and the radar moving speed on rail is limited as 0.03 m/s, which is slower than most moving targets. The rail length of the radar is 0.8 m. The signal bandwidth is 400 MHz. The maximum illuminating range is 2500 m to 5000 m. Here, we used 2500 m as simulation parameter. Since the NCUT risk radar uses the transmitted signal for pulse compression, the reference range ($R_{ref)}$ is zero. The Pulse Repetition Frequency (PRF) is set 500 Hz.

Table 1. Radar parameters.

Parameter	Value	Parameter	Value
Center frequency	17 GHz	PRF	500 Hz
Signal bandwidth	400 MHz	Near range	500 m
Radar speed	0.03 m/s	Far range	2500 m
Pulse duration	0.002 s	Rail length	0.8 m

Table 2 shows the parameters of targets in experiment. T1, T2, T3 and T4 are moving targets, and S1 is the stationary target for comparison. The simulation includes two cases. The difference is that the position component y is 0 or not when azimuth time t_{azi} is 0. According to Chinese regulation of safe production in mining areas, the maximum driving speed is less than 30 km/h (8.3 m/s) [35]. Thus, target maximum speed set in experiment is 10 m/s.

Table 2. Target parameters.

Target	Coordinate [m]	Vr [m/s]	Va [m/s]
S1	(1850, 0)	0	0
T1	(2000, 0)	0	10
T2	(2050, 100)	0	10
T3	(2200, 0)	2	5
T4	(2300, 100)	2	2

The stationary reference point S1 is located at (1850 m, 0). After GBSAR imaging, it can be seen from the Figure 6. S1 is well focused. Moving targets T1 and T2 are defocused and T3 and T4 are defocused and displaced.

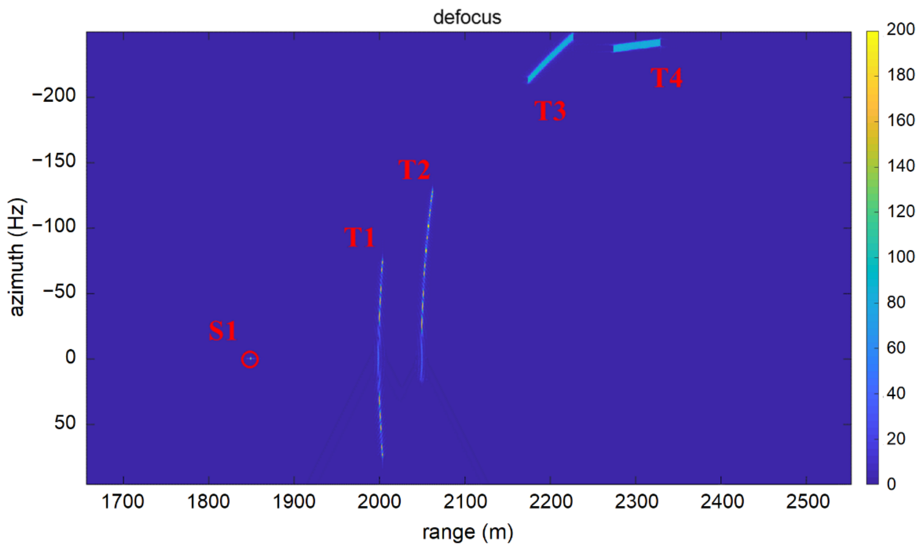

Figure 6. The defocused image without refocus processing.

Case 1: target position y = 0 at t_{azi} = 0

When $t_{azi} = 0$, the moving targets T1 and T3 are located at (2000 m, 0) and (2200 m, 0), respectively. The motion parameters of T1 are $v_r = 0$ m/s and $v_a = 10$ m/s, and the motion parameters of T3 are $v_r = 2$ m/s and $v_a = 5$ m/s. According to Equation (6) in Section 2, the relative speed v_s' of T1 and T3 are −9.97 m/s and −5.35 m/s, respectively. Their refocusing result is shown in Figure 7. The T3 is taken as an example to analyze refocusing quality.

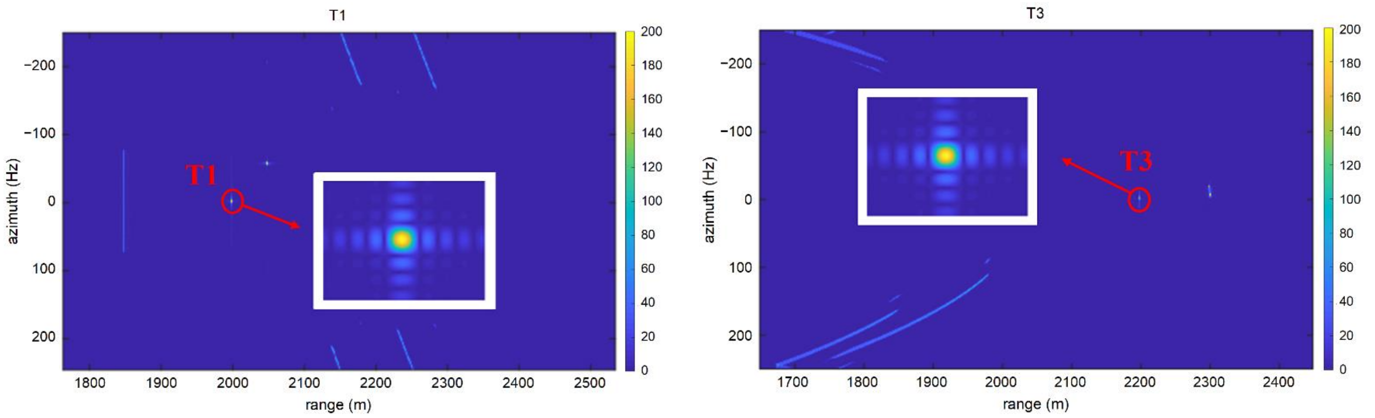

Figure 7. Refocused result of the moving targets T1 and T3.

The impulse responses of T3 and the azimuth and range profiles are shown in Figure 8. The Peak Side-Lobe Ratio (PSLR) and Integration Side-Lobe Ratio (ISLR) are used as criteria, and their theoretical values are around −13.26 dB (PSLR) and −9.80 dB (ISLR), respectively [36]. The PSLR and ISLR of the refocused image in the range direction are −13.3 dB and −10.6 dB. The PSLR and ISLR of the refocused image in the azimuth direction are −12.5 dB and −9.1 dB, respectively. It can be seen that evaluated parameters agree with the theoretical values, which means the algorithm can achieve good refocusing results.

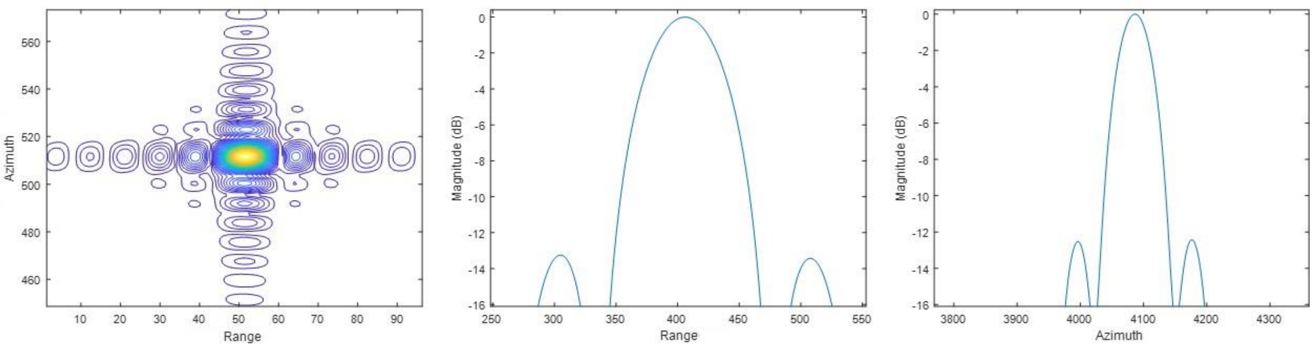

(**a**) (**b**) (**c**)

Figure 8. Refocused result of the moving target T3. (**a**) Impulse responses of T3. (**b**) Range profile of T3. (**c**) Azimuth profile of T3.

Figure 9 shows the comparison before and after the refocusing of T1. After considering the motion characteristics of the moving target, the 2D parameters search space (v'_s, θ') is established for T1, and the refocusing is performed. It can be seen from the figure that T1 changes from the original defocusing state to the focusing state. Additionally, the original focused static point S1 becomes defocusing. So, for different targets, the matched values of v'_s and θ' are different. Only the moving target that matches the parameters in iteration can be refocused. The other targets become defocusing due to the relative speed parameters' mismatch. Therefore, the refocusing algorithm processes the target by target via searching 2D parameters space.

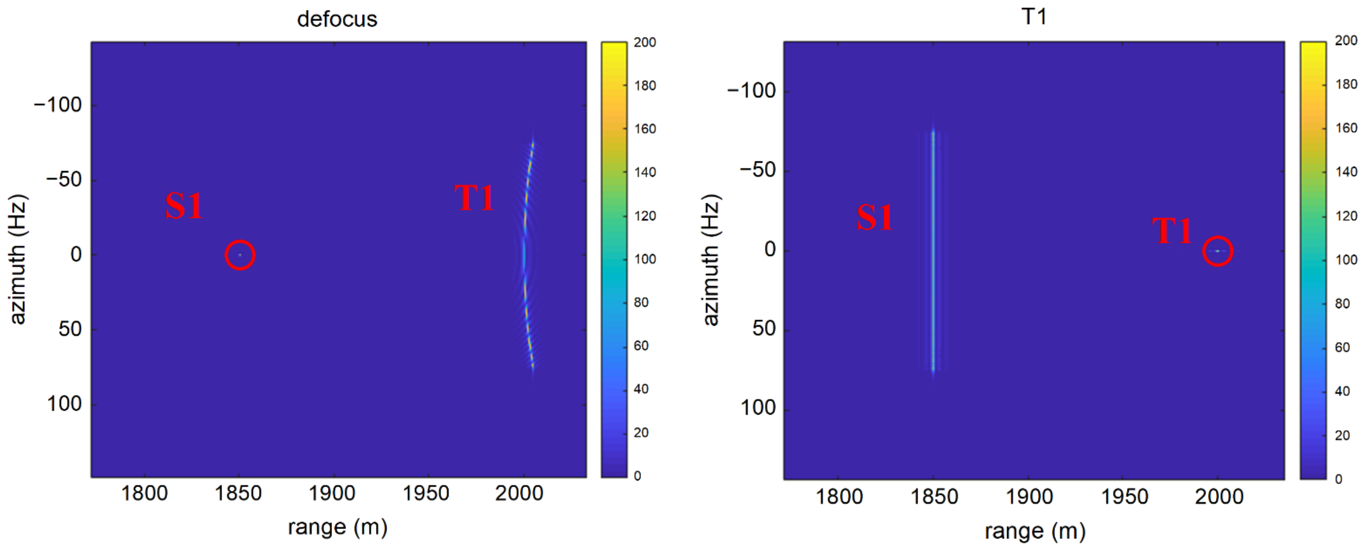

Figure 9. Comparison before and after the refocused of T1.

Case 2: target position y $\neq$ 0 at t_{azi} = 0

The moving targets T2 and T4 are located at (2050 m, 100 m) and (2300 m, 100 m) when $t_{azi} = 0$, respectively. The motion parameters of T2 are v_r =0 m/s and v_a =10 m/s, and the motion parameters of T4 are v_r =2 m/s and v_a =2 m/s. The relative speeds v_s' are −9.97 m/s and −2.80 m/s, respectively. Their refocusing result is shown in Figure 10. Similar to that in case 1, take the T4 as an example to analyze the refocusing quality. The impulse responses of T4 and the azimuth and range profiles are shown in Figure 11. The PSLR and ISLR of the refocused image in the range direction are −13.4 dB and −10.7 dB. The PSLR and ISLR of the refocused image in the azimuth direction are −13.2 dB and −9.6 dB, respectively.

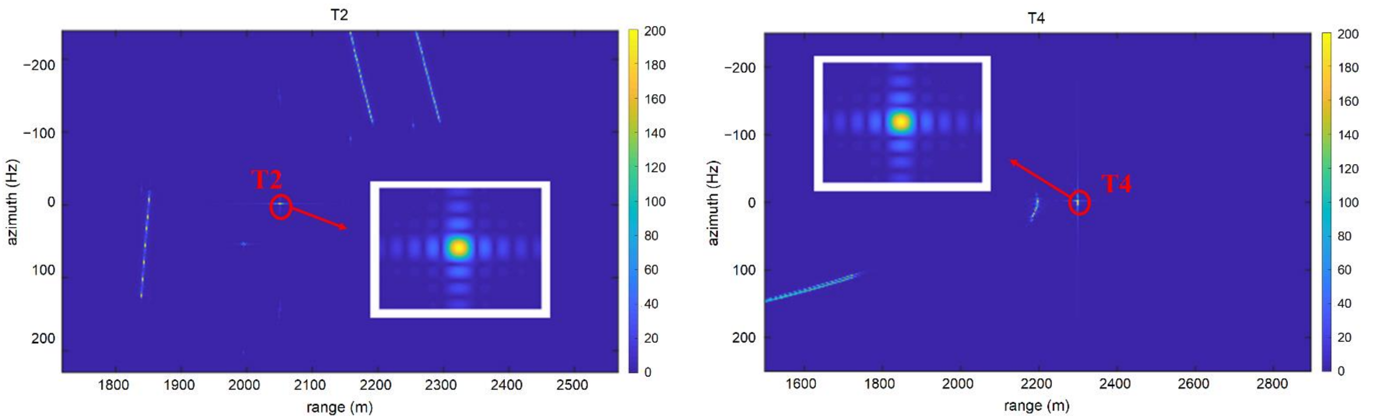

Figure 10. Refocused result of the moving target T2 and T4.

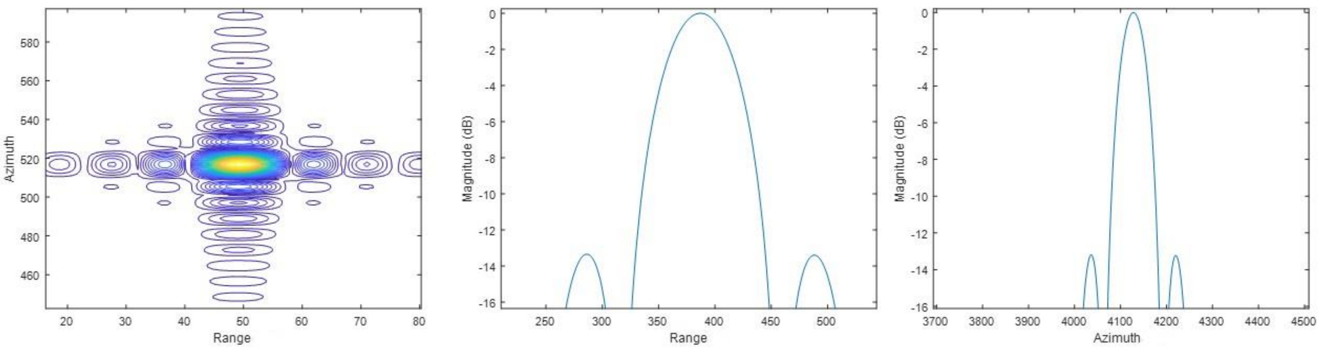

(**a**) (**b**) (**c**)

Figure 11. Refocused result of the moving target T4. (**a**) Impulse responses of T4. (**b**) Range profile of T4. (**c**) Azimuth profile of T4.

The above cases validate the proposed algorithm.

5.2. Synthetic Data

This section describes the synthetic data experiment which combines the real data acquired in mine and simulated moving target echo. The real data is collected by NCUT-RiskRadar GBSAR system. Figure 12 shows the photo of GBSAR system, its parameters are same as shown previously in Table 1. Two targets, A1 and A2, are simulated, and the positions are (1900 m, 0 m) and (2000 m, 50 m) when azimuth time is 0. The range and azimuth speed of A1 and A2 are (0, 3) m/s and (0, 2) m/s. Table 3 shows the target parameters of synthetic data.

Figure 12. The NCUT Risk Radar GBSAR System.

Table 3. Target parameters of synthetic data.

Target	Coordinate [m]	Vr [m/s]	Va [m/s]
A1	(1900, 0)	0	3
A1	(2000, 50)	0	2

The synthesized image is shown in Figure 13, and the image of mine area is located at the middle. A1 and A2 are labeled with a red dashed box. Apply the proposed method to the two targets, A1 and A2 before and after refocusing are shown in Figure 14. In the local image, we can find that the stationary scene is well focused and the targets are defocused. When imaging iteratively using different 2D parameters, the targets getting focused and the scene is defocused.

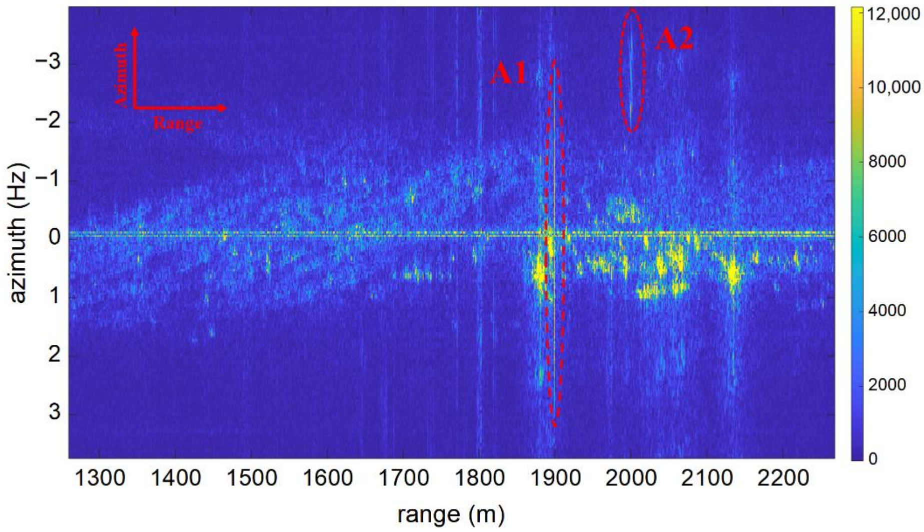

Figure 13. The imaging result of the synthetic data.

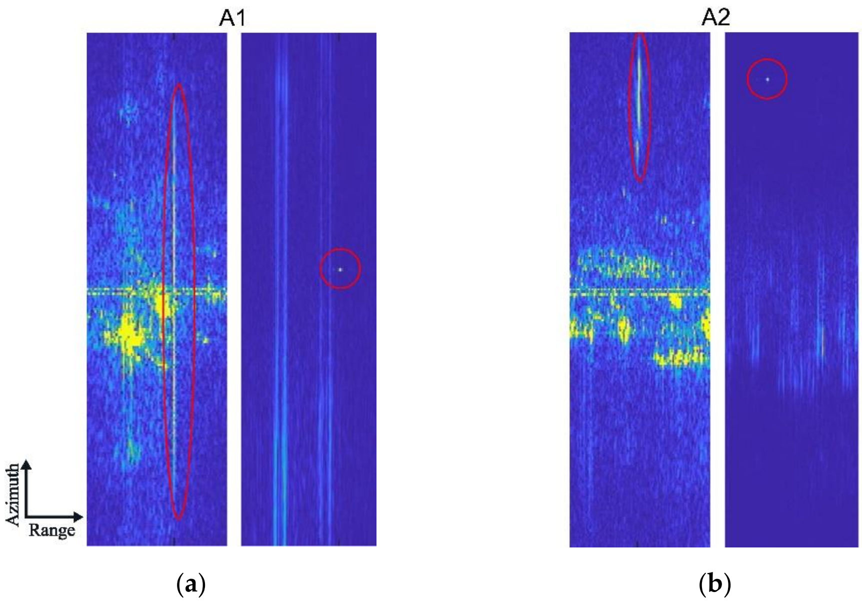

Figure 14. Comparison of imaging results of two ground moving targets before and after refocusing. (**a**) Imaging results of A1 before and after refocusing. (**b**) Imaging results of A2 before and after refocusing.

Thus, the effectiveness of proposed method in data contain real scene is validated.

6. Conclusions

In this paper, a single-channel FMCW-GBSAR moving target refocusing imaging algorithm based on relative speed is proposed. The FMCW-GBSAR moving target signal model is firstly analyzed. Then, the relative speed signal model is deduced. Based on this model and the incomplete synthetic aperture of GBSAR, the Range Doppler (RD) algorithm is adopted and improved in this paper. The algorithm is controlled by relative speed and squint angle; thus, the refocused target image can be obtained via searching 2D parameters. By introducing the relative speed, the original complex moving target signal model is simplified to the same form as the stationary signal model. The existing imaging algorithms can be fully utilized to reduce the difficulty of algorithm modification. The proposed method is verified by the synthetic data, which are generated by combining NCUT FMCW GBSAR real data and simulated moving target echo.

The future works includes conducts the real FMCW-GBSAR moving target experiment, and studies and optimizes the 2D parameters searching strategy. Additionally, study moving targets suppress method based on the proposed refocusing method for GBSAR.

Author Contributions: Conceptualization, W.S.; methodology, W.S. and S.W.; software, W.S. and S.W.; validation, W.S. and S.W.; formal analysis, W.S. and S.W.; resources, Y.L. (Yun Lin) and Y.L. (Yang Li); writing—original draft preparation, W.S. and S.W.; writing—review and editing, W.S., S.W., Y.L. (Yun Lin), Y.L. (Yang Li), F.D. and Y.W.; supervision, Y.W.; project administration, Y.W.; funding acquisition, Y.W. All authors have read and agreed to the published version of the manuscript.

Funding: This research was funded by Innovation Team Building Support Program of Beijing Municipal Education Commission, grant number IDHT20190501; the Fundamental Research Fund of Beijing Municipal Education Commission, grant number 110052972027/119; R&D Program of Beijing Municipal Education Commission, grant number KM202210009004; North China University of Technology Research start-up Funds, grant number 110051360002; National Natural Science Foundation of China Grant 62131001.

Data Availability Statement: Not applicable.

Acknowledgments: We thank the good advice and comments from anonymous reviewers to help improve the quality of the paper.

Conflicts of Interest: The authors declare no conflict of interest.

Appendix A

Recall the expression of $R(0)$,$R'(0)$ and $R''(0)$; if they are substituted into Equation (5), the expression of moving target signal in GBSAR is as follows:

$$
\begin{aligned}
s(t_r,t_a) \quad &= A_0 \cdot \exp\left(-j\frac{4\pi}{\lambda}\left(\sqrt{x_0^2+y_0^2}+\frac{\left(\left(v_r^2+(v_a-v_s)^2\right)\cdot(x_0^2+y_0^2)^{-\frac{1}{2}}-(x_0^2v_r^2+y_0^2(v_a-v_s)^2)\cdot\left(x_0^2+y_0^2\right)^{-\frac{3}{2}}\right)}{2}t_a^2\right)\right)\cdot\exp\left(j\frac{4\pi}{\lambda}\cdot\left(\left(x_0^2+y_0^2\right)^{-\frac{1}{2}}\cdot(v_rx_0+(v_a-v_s)y_0)\right)\cdot t_r\right) \\
&\exp\left(-j\frac{4\pi}{\lambda}\cdot\left(\left(v_r^2+(v_a-v_s)^2\right)\cdot(x_0^2+y_0^2)^{-\frac{1}{2}}-(x_0^2v_r^2+y_0^2(v_a-v_s)^2)\cdot\left(x_0^2+y_0^2\right)^{-\frac{3}{2}}\right)\cdot t_rt_a\right)\cdot\exp\left(j\frac{4\pi}{\lambda}\cdot\left(\left(x_0^2+y_0^2\right)^{-\frac{1}{2}}\cdot(v_rx_0+(v_a-v_s)y_0)\right)\cdot t_a\right)\cdot \\
&\exp\left[-j\frac{4\pi}{c}K_r\left(\sqrt{x_0^2+y_0^2}+\left(\left(x_0^2+y_0^2\right)^{-\frac{1}{2}}\cdot(v_rx_0+(v_a-v_s)y_0)\right)\cdot t_a+\frac{\left(\left(v_r^2+(v_a-v_s)^2\right)\cdot(x_0^2+y_0^2)^{-\frac{1}{2}}-(x_0^2v_r^2+y_0^2(v_a-v_s)^2)\cdot\left(x_0^2+y_0^2\right)^{-\frac{3}{2}}\right)}{2}\cdot t_a^2-R_{ref}\right)\left(t_r-\frac{2R_{ref}}{c}\right)\right]\cdot \\
&\exp\left[j\frac{4\pi K_r}{c^2}\left(\left(v_r^2+(v_a-v_s)^2\right)\cdot(x_0^2+y_0^2)^{-\frac{1}{2}}-(x_0^2v_r^2+y_0^2(v_a-v_s)^2)\cdot\left(x_0^2+y_0^2\right)^{-\frac{3}{2}}-R_{ref}\right)^2\right]
\end{aligned}
\tag{A1}
$$

References

1. Liu, B.; Ge, D.; Li, M.; Zhang, L.; Wang, Y.; Zhang, X. Using GB-SAR technique to monitor displacement of open pit slope. In Proceedings of the 2016 IEEE International Geoscience and Remote Sensing Symposium (IGARSS), Beijing, China, 10–15 July 2016; pp. 5986–5989.
2. Tarchi, D.; Casagli, N.; Fanti, R.; Leva, D.D.; Luzi, G.; Pasuto, A.; Pieraccini, M.; Silvano, S. Landslide monitoring by using ground-based SAR interferometry: An example of application to the Tessina landslide in Italy. *Eng. Geol.* **2003**, *68*, 15–30. [CrossRef]
3. Perry, R.P.; Dipietro, R.C.; Fante, R.L. SAR imaging of moving targets. *IEEE Trans. Aerosp. Electron. Syst.* **1999**, *35*, 188–200. [CrossRef]
4. Zhou, F.; Wu, R.; Xing, M.; Bao, Z. Approach for single channel SAR ground moving target imaging and motion parameter estimation. *IET Radar Sonar Navig.* **2007**, *1*, 59–66. [CrossRef]
5. Zhu, D.; Li, Y.; Zhu, Z. A keystone transform without interpolation for SAR ground moving-target imaging. *IEEE Geosci. Remote Sens. Lett.* **2007**, *4*, 18–22. [CrossRef]
6. Li, G.; Xia, X.-G.; Peng, Y.-N. Doppler keystone transform: An approach suitable for parallel implementation of SAR moving target imaging. *IEEE Geosci. Remote Sens. Lett.* **2008**, *5*, 573–577. [CrossRef]
7. Sun, G.; Xing, M.; Xia, X.-G.; Wu, Y.; Bao, Z. Robust ground moving-target imaging using deramp–keystone processing. *IEEE Geosci. Remote Sens.* **2012**, *51*, 966–982. [CrossRef]
8. Zhu, S.; Liao, G.; Qu, Y.; Zhou, Z.; Liu, X. Ground moving targets imaging algorithm for synthetic aperture radar. *IEEE Geosci. Remote Sens.* **2010**, *49*, 462–477. [CrossRef]
9. Jao, J.K. Theory of synthetic aperture radar imaging of a moving target. *IEEE Geosci. Remote Sens.* **2001**, *39*, 1984–1992. [CrossRef]

10. Dong, Q.; Xing, M.-D.; Xia, X.-G.; Zhang, S.; Sun, G.-C. Moving target refocusing algorithm in 2-D wavenumber domain after BP integral. *IEEE Geosci. Remote Sens. Lett.* **2017**, *15*, 127–131. [CrossRef]
11. Sjogren, T.K.; Vu, V.T.; Pettersson, M.I.; Gustavsson, A.; Ulander, L.M.H. Moving target relative speed estimation and refocusing in synthetic aperture radar images. *IEEE Trans. Aero. Elec. Syst.* **2012**, *48*, 2426–2436. [CrossRef]
12. Vu, V.T.; Pettersson, M.I.; Sjögren, T.K. Moving target focusing in SAR image with known normalized relative speed. *IEEE Trans. Aero. Elec. Sys.* **2017**, *53*, 854–861. [CrossRef]
13. Wan, J.; Zhou, Y.; Zhang, L.; Chen, Z.; Yu, H. Efficient Algorithm for SAR Refocusing of Ground Fast-Maneuvering Targets. *Remote Sens.* **2019**, *11*, 2214. [CrossRef]
14. Shu, Y.; Wan, J.; Li, D.; Chen, Z.; Liu, H. Fast Approach for SAR Imaging of Ground-Based Moving Targets Based on Range Azimuth Joint Processing. *Remote Sens.* **2022**, *14*, 2965. [CrossRef]
15. Meta, A.; Hoogeboom, P.; Ligthart, L.P. Signal Processing for FMCW SAR. *IEEE Geosci. Remote Sens.* **2007**, *45*, 3519–3532. [CrossRef]
16. de Wit, J.J.M.; Meta, A.; Hoogeboom, P. Modified range-Doppler processing for FM-CW synthetic aperture radar. *IEEE Geosci. Remote Sens. Lett.* **2006**, *3*, 83–87. [CrossRef]
17. Meta, A.; Hoogeboom, P.; Ligthart, L.P. Non-linear Frequency Scaling Algorithm for FMCW SAR Data. In Proceedings of the 2006 European Radar Conference, Manchester, UK, 13–15 September 2006; pp. 9–12.
18. Guarnieri, A.M.; Scirpoli, S. Efficient wavenumber domain focusing for ground-based SAR. *IEEE Geosci. Remote Sens. Lett.* **2009**, *7*, 161–165. [CrossRef]
19. Guo, S.; Dong, X. Modified Omega-K algorithm for ground-based FMCW SAR imaging. In Proceedings of the 2016 IEEE 13th International Conference on Signal Processing (ICSP), Chengdu, China, 6–10 November 2016; pp. 1647–1650.
20. Yuan, Z.; Qiming, Z.; Yanping, W.; Yun, L.I.N.; Yang, L.I.; Zechao, B.A.I.; Fang, L.I. An approach to wide-field imaging of linear rail ground-based SAR in high squint multi-angle mode. *J. Syst. Eng. Electron.* **2020**, *31*, 722–733. [CrossRef]
21. Zhang, Y.; Sun, J.; Lei, P.; Li, G.; Hong, W. High-resolution SAR-based ground moving target imaging with defocused ROI data. *IEEE Trans. Geosci. Remote Sens.* **2015**, *54*, 1062–1073. [CrossRef]
22. Jiang, Z.-H.; Huang-Fu, K.; Wan, J.-W. A chirp transform algorithm for processing squint mode FMCW SAR data. *IEEE Geosci. Remote Sens. Lett.* **2007**, *4*, 377–381. [CrossRef]
23. Wang, R.; Loffeld, O.; Nies, H.; Knedlik, S.; Hagelen, M.; Essen, H. Focus FMCW SAR data using the wavenumber domain algorithm. *IEEE Trans. Geosci. Remote Sens.* **2009**, *48*, 2109–2118. [CrossRef]
24. Ribalta, A. Time-domain reconstruction algorithms for FMCW-SAR. *IEEE Trans. Geosci. Remote Sens. Lett.* **2010**, *8*, 396–400. [CrossRef]
25. Cheng, P.; Xin, Q.; Wan, J.; Wang, Z. Refocusing of ground moving targets for range migration algorithm in FMCW SAR. In Proceedings of the SAR Image Analysis, Modeling, and Techniques XV, Toulouse, France, 15 October 2015; p. 96420R.
26. Zhang, H.; Ni, J.; Xiong, S.; Luo, Y.; Zhang, Q. Omega-KA-Net: A SAR Ground Moving Target Imaging Network Based on Trainable Omega-K Algorithm and Sparse Optimization. *Remote Sens.* **2022**, *14*, 1664. [CrossRef]
27. Casalini, E.; Frioud, M.; Small, D.; Henke, D. Refocusing FMCW SAR moving target data in the wavenumber domain. *IEEE Geosci. Remote Sens.* **2019**, *57*, 3436–3449. [CrossRef]
28. Meta, A.; Hoogeboom, P.; Ligthart, L.P. Correction of the effects induced by the continuous motion in airborne FMCW SAR. In Proceedings of the 2006 IEEE Conference on Radar, Verona, NY, USA, 24–27 April 2006; p. 8.
29. Liang, Y.; Wang, H.; Xing, M.; Bao, Z. Imaging Study of High Squint SAR Based on FMCW. In Proceedings of the 2007 1st Asian and Pacific Conference on Synthetic Aperture Radar, Huangshan, China, 5–9 November 2007; pp. 6–9.
30. Liang, X.; Wei, Q. Wavenumber domain algorithm for squint FMCW SAR. In Proceedings of the 2011 6th International Forum on Strategic Technology, Harbin, China, 22–24 August 2011; pp. 1256–1260.
31. Liang, Y.; Wang, H.X.; Xing, M.D.; Bao, Z. Slow ground moving target parameter estimation and imaging in FMCW SAR. *Syst. Eng. Electr.* **2011**, *33*, 1001–1006. [CrossRef]
32. Bao, Z.; Xing, M.D.; Wang, T. *Radar Imaging Techniques*; Publishing House of Electronics Industry: Beijing, China, 2006.
33. Meta, A.; Hoogeboom, P. Signal processing algorithms for FMCW moving target indicator synthetic aperture radar. In Proceedings of the 2005 IEEE International Geoscience and Remote Sensing Symposium, 2005. IGARSS '05., Seoul, Korea, 29 July 2005; p. 4.
34. Liang, Y.; Wang, H.-X.; Xing, M.-D.; Bao, Z. The analysis of FMCW SAR signal and image study. *J. Electr. Inform. Technol.* **2008**, *30*, 1017–1021. [CrossRef]
35. State Administration of Work Safety. *National Mine Safety Administration. Coal Mine Safety Code*; China Coal Industry Publishing House: Beijing, China, 2016.
36. Tang, S.; Zhang, L.; Guo, P.; Liu, G.; Sun, G.C. Acceleration Model Analyses and Imaging Algorithm for Highly Squinted Airborne Spotlight-Mode SAR with Maneuvers. *IEEE J. Sel. Top. Appl. Earth Obs. Remote Sens.* **2015**, *8*, 1120–1131. [CrossRef]